ISA Transactions 158 (2025) 62–72

Contents lists available at ScienceDirect

ISA Transactions

journal homepage: www.elsevier.com/locate/isatrans

Research article

Event-triggered adaptive compensation control for stochastic nonlinear systems with multiple failures: An improved switching threshold strategy ☆

Yang Du [a], Shan-Liang Zhu [a,b,c], Yu-Qun Han [a,b,c,*]

[a] School of Mathematics and Physics, Qingdao University of Science and Technology, Qingdao 266061, China
[b] Qingdao Innovation Center of Artificial Intelligence Ocean Technology, Qingdao 266061, China
[c] The Research Institute for Mathematics and Interdisciplinary Sciences, Qingdao University of Science and Technology, Qingdao 266061, China

ARTICLE INFO

Keywords:
Event-triggered control
Stochastic nonlinear systems
Fault-tolerant control
Adaptive control

ABSTRACT

This paper considers the event-triggered adaptive fault-tolerant control (FTC) problem for a class of stochastic nonlinear systems suffering from finite number of actuator failures and abrupt system external failure. Unlike existing event-triggered mechanisms (ETMs), this paper proposes an improved switching threshold mechanism (STM) that effectively addresses the potential system security hazards caused by large signal impulses when both the magnitude size of the controller and its rate of change are too large, while also saving energy consumption. Especially, when the occurrence of both actuator failure and system external failure may lead to over-change rate of the controller, by using the multi-dimensional Taylor network (MTN) approximation technique, the adaptive fault-tolerant control scheme designed based on the improved STM not only has lower resource consumption, but also indirectly improves the control performance of the system by ensuring the system security operation. Not only does it ensure that all signals of the closed-loop system are bounded in probability and the tracking error converges through the proposed control scheme. The feasibility and superiority of the developed scheme is well shown by dynamic model simulations.

1. Introduction

In practical engineering, many systems, such as robotic systems, electric power systems, satellite control systems, and unmanned aerial vehicle control systems, are inherently nonlinear. Consequently, ensuring the stability of nonlinear systems is of paramount importance, and a variety of control methods have been proposed, including adaptive backstepping control [1], robust control [2], sliding mode control [3], and optimal control [4]. In recent years, with the increasing demand for higher system control accuracy, the impact of stochastic disturbances has become more significant, prompting extensions of these traditional methods to accommodate stochastic nonlinear systems [5–7]. Despite these advances, adaptive backstepping control remains limited in its ability to handle strong system nonlinearities and uncertainties.

To address this limitation, intelligent control methods – such as neural networks (NNs) [8,9], fuzzy logic systems (FLSs) [10], and multi-dimensional Taylor networks (MTNs) [11] – have been increasingly employed, leveraging approximation techniques to design more robust control strategies for stochastic nonlinear systems. The MTN-based control methods, in particular, stand out for their ability to simplify control structures and alleviate computational complexity, making them ideal for applications in nonlinear, switching, and stochastic nonlinear systems [12–14].

Simultaneously, networked control systems (NCSs) have garnered significant attention due to their wide-ranging applications in fields such as telemedicine, wireless communications, aerospace, and automotive systems. In NCSs, system components (e.g., sensors, controllers, actuators) communicate via a shared network, where bandwidth and computational power limitations pose challenges to performance. Event-triggered control (ETC) strategies, which intermittently send quantized control signals to actuators, offer a promising solution by reducing communication overhead and computational demands. Event-triggered mechanisms (ETMs) generally fall into three types: fixed threshold [15], relative threshold [16,17], and switching threshold [18,19]. However, these mechanisms have limitations: the fixed threshold mechanism (FTM) is simplistic and can lead to conservative control performance; the relative threshold mechanism (RTM) can result in excessively long update intervals and potential instability, especially when control signals vary rapidly. Moreover, large amplitude fluctuations in the control signal can lead to unsafe impulses, jeopardizing system reliability.

☆ This work was supported by the Shandong Provincial Natural Science Foundation, China (No. ZR2020QF055).
* Corresponding author at: School of Mathematics and Physics, Qingdao University of Science and Technology, Qingdao 266061, China.
E-mail addresses: 2021090004@mails.qust.edu.cn (Y. Du), zhushanliang@qust.edu.cn (S.-L. Zhu), yuqunhan@qust.edu.cn (Y.-Q. Han).

https://doi.org/10.1016/j.isatra.2025.01.024
Received 4 January 2024; Received in revised form 11 January 2025; Accepted 11 January 2025
Available online 20 January 2025

The conventional switching threshold mechanism (STM) combines elements of both the FTM and the RTM to balance security and precision. However, it fails to adequately address the risks posed by excessive controller change rates, which can lead to significant system safety hazards. Thus, there is a pressing need for an improved STM that considers both the controller's amplitude and its rate of change to ensure system safety without compromising performance.

In practical NCSs, control signals are transmitted to plants through actuators. However, as the complexity of NCSs increases, actuators are prone to experiencing partial loss of effectiveness (PLOE) or total loss of effectiveness (TLOE) during operation. To mitigate the impact of actuator failures, various failure-tolerant control (FTC) strategies have been proposed for different system types, including nonlinear multi-agent systems [20,21], uncertain nonlinear systems [22,23], and large-scale nonlinear systems [24,25]. Recent studies, such as those by Pan et al. [26] and Wang et al. [27], have developed FTC schemes within the framework of the RTM. These schemes offer the advantage of extending update intervals through larger measurement errors when actuator failures occur, thereby reducing communication overhead. However, this strategy fails to address a critical issue: the potential for large overload impulses, arising from long update intervals and excessive rates of change in the actuator and controller signals, which can severely compromise system safety and stability.

Moreover, the consideration of abrupt system external failure in [28] highlights additional security risks within the RTM framework, which are further compounded when both actuator failures and abrupt system external failure occur simultaneously, as discussed in [29,30]. Despite these advancements, the conventional STM remains inadequate in accounting for the security hazards posed by excessive rates of change in control signals. This underscores a crucial gap in the existing literature: the need for an ETM that not only accommodates multiple failure scenarios but also explicitly considers the impact of the controller's rate of change on the overall system security. Addressing this gap is vital for enhancing the robustness and reliability of NCSs, particularly in failure-prone environments.

Motivated by these challenges, this paper proposes a novel approach that integrates multiple failure scenarios (including actuator failures and system external failure) into the event-triggered framework. Specifically, the contributions of this paper are twofold:

(1) Unlike previous studies [29,30] that primarily address single actuator failures or isolated system external failures, this paper extends the failure-tolerant framework to encompass multiple actuator failures and system resource constraints. This extension provides a more accurate representation of real-world engineering applications, where multiple failure modes can occur simultaneously. Leveraging the MTN approximation technique, we propose a new event-triggered FTC scheme that not only compensates for the effects of these failures but also minimizes energy consumption. The MTN-based controller is characterized by its simplified structure, which reduces computational complexity and resource demands, thereby enhancing control efficiency while maintaining robustness in the presence of system failures.

(2) Building upon the conventional STM, we introduce an improved STM that simultaneously considers both the magnitude and the rate of change of the control signal. This integrated approach mitigates the risk of large, destabilizing impulses that can arise from rapid variations in control inputs, thus ensuring improved system safety and stability. At the same time, it achieves significant communication and computational resource savings by more efficiently triggering control updates. This novel mechanism addresses the limitations of traditional ETMs by providing a more comprehensive solution to system safety under dynamic and failure-prone conditions.

The main structure of the paper is as follows: Section 2 introduces the definition of symbols, system description, actuator failure model, control aims, stochastic system theory, MTN approximation principle, and necessary definitions, lemmas, and assumptions; Section 3 provides the main research results of this paper, including the design of the event-triggered adaptive fault-tolerant controller, the proof of system stability, and the avoidance of Zeno behavior; The effectiveness and superiority of the proposed control scheme are verified in Section 4 through simulation research on the 3-order single-link manipulator dynamic model, while Section 5 summarized this paper.

2. Problem statement and preliminaries

Notations. In this paper, the arguments of the functions are omitted or simplified whenever no confusion can arise from the context. For example, we may denote $f_j\left(\bar{\chi}_j\right)$, $F_j\left(\boldsymbol{Z}_j\right)$ and $S_{m_n}\left(\boldsymbol{Z}_j\right)$ by f_j, F_j and S_{m_j}, respectively. R^r denotes the real r-dimensional Euclidean space. $R^{n\times r}$ denotes the real $n\times r$ matric space. N^* represents the set of all positive integers. $|X|$ denotes the absolute value of the real number X. $\|\boldsymbol{X}\|$ denotes the Euclidean norm of vector $\boldsymbol{X}$. X^{T} represents the transpose of vector X. $E(\cdot)$ denotes Expectation operator symbol. $\mathrm{Tr}\{\Delta\}$ is the trace of matrix Δ. C^i denotes the set with ith partial derivative functions. $\mathrm{sign}(\cdot)$ denotes the normal sign function. $\tanh(\cdot)$ represents the hyperbolic tangent function.

2.1. System and model statement

The stochastic nonlinear system considered in this paper with the following form

$$\begin{cases} d\chi_j = \left(f_j\left(\bar{\chi}_j\right) + \chi_{j+1}\right)dt + \phi_j^{\mathrm{T}}\left(\bar{\chi}_j\right)d\vartheta \\ \quad j = 1,2,\ldots,n-1 \\ d\chi_n = \left(f_n\left(\bar{\chi}_n\right) + \mu(t) + \Gamma(t)\,\mathrm{P}(\chi)\right)dt \\ \qquad + \phi_n^{\mathrm{T}}\left(\bar{\chi}_n\right)d\vartheta \\ \quad y = \chi_1 \\ \mu(t) = \sum_{i=1}^{w} c_i\varphi_i(\chi)\,\mu_{bi}(t) \end{cases} \tag{1}$$

where $\mu_{bi}(t)\in R$, $\mu(t)\in R$ and $y\in R$ represent the ith actuator output, system input and output, respectively. $\chi = [\chi_1,\chi_2,\ldots,\chi_n]^{\mathrm{T}}\in R^n$ is system state vector with $\bar{\chi}_j = [\chi_1,\chi_2,\ldots,\chi_j]^{\mathrm{T}}\in R^j, j = 1,2,\ldots,n$. $f_j(\cdot)\in R$ and $\phi_j(\cdot)\in R^r$ stand for the unknown smooth nonlinear functions with $f_j(\mathbf{0}) = 0$ and $\phi_j(\mathbf{0}) = \mathbf{0}$; $\varphi_i(\chi)(i = 1,2,\ldots,w)$ and $c_i\in R$ are known smooth nonlinear function and unknown constant, respectively; ϑ is an r-dimensional standard Wiener process. $\mathrm{P}(\chi)$ is an unknown function representing the system external failure. The diagonal matrix $\Gamma(t)$ is designed as

$$\Gamma(t) = \begin{cases} 1, & t\geq T_F \\ 0, & t < T_F \end{cases} \tag{2}$$

where T_F denotes the time when the external failure starts at the system.

We consider the ith actuator that may fail during the operation, and its failure model at time instant t_{Fi} is formulated as

$$\mu_{bi}(t) = \lambda_i\mu_{PFi}(t) + \mu_{TFi}, \forall t\geqslant t_{Fi} \tag{3}$$

where ith actuator input is $\mu_{PFi}(t)$ and output is $\mu_{bi}(t)$. $\lambda_i\in[0,1)$, t_{Fi} and $\mu_{TFi}(t)$ are unknown constants. Therefore, two patterns of actuator failures are considered as follows.

(1) PLOE. That is to say, the output $\mu_{bi}(t)$ of the actuator loses some of its performance, i.e., $\mu_{bi}(t) = \lambda_i\mu_{PFi}(t)$, $\lambda_i\in(0,1)$ and $\mu_{TFi} = 0$.

(2) TLOE. That is to say, the output $\mu_{bi}(t)$ of the actuator will be affected by μ_{TFi}, not $\mu_{PFi}(t)$, i.e., $\mu_{bi}(t) = \mu_{TFi}$, $\lambda_i = 0$.

It should be noted that the actuator operates in failure-free case can still be expressed as (3) with $\lambda_i = 1$ and $\mu_{TFi} = 0$. Therefore, the model in (3) is suitable for describing the output of the actuator, regardless of whether it fails.

According to the above failure model, the system (1) can be reformulated as

$$\begin{cases} d\chi_j = \left(f_j\left(\bar{\chi}_j\right) + \chi_{j+1}\right) dt + \phi_j^{\mathrm{T}}\left(\bar{\chi}_j\right) d\vartheta \\ \quad j = 1, 2, \ldots, n-1 \\ d\chi_n = \left(f_n\left(\bar{\chi}_n\right) + \sum_{i=1}^{w} c_i \varphi_i(\chi)\left(\lambda_i \mu_{PFi}(t) + \mu_{TFi}\right)\right. \\ \qquad \left. + \Gamma(t)\,\mathrm{P}(\chi)\right) dt + \phi_n^{\mathrm{T}}\left(\bar{\chi}_n\right) d\vartheta \\ y = \chi_1 \end{cases} \tag{4}$$

Remark 1. It is crucial to underscore that system (4) has the capability to represent a broader spectrum of faults, including lock-in-place (LIP) fault, float fault, and hard-over fault, as referenced in [31,32]. Contrary to the extensively researched fault-tolerant control strategies for nonlinear systems [31,32], this study specifically targets event-triggered adaptive compensation control strategy for stochastic nonlinear systems experiencing loss of effectiveness faults, encompassing both PLOE and TLOE.

In practical systems, the communication between controllers and actuators is implemented through a shared network. However, in the control design process of most systems, network resource is usually assumed to be sufficient, but it is limited. Thereby, an improved STM between the ith controller and the ith actuator is considered as

$$\begin{cases} \mu_{PFi}(t) = \varpi_i\left(t_k\right), \forall t \in \left[t_k, t_{k+1}\right) \\ t_{k+1} = \begin{cases} \inf\left\{t \in R \mid |e(t)| \geqslant \mathrm{M}_1\right\}, \\ \qquad \left|\dot{\varpi}_i(t)\right| > \mathrm{T}_1 \\ \inf\left\{t \in R \mid |e(t)| \geqslant \mathrm{M}_2\right\}, \\ \qquad \left|\mu_{PFi}(t)\right| > \mathrm{T}_2, \left|\dot{\varpi}_i(t)\right| \leqslant \mathrm{T}_1 \\ \inf\left\{t \in R \mid |e(t)| \geqslant \zeta\left|\mu_{PFi}(t)\right| + \mathrm{M}_3\right\}, \\ \qquad \left|\mu_{PFi}(t)\right| \leqslant \mathrm{T}_2, \left|\dot{\varpi}_i(t)\right| \leqslant \mathrm{T}_1 \end{cases} \end{cases} \tag{5}$$

where $e(t) = \varpi_i(t) - \mu_{PFi}(t)$ represents the measurement error, $\mathrm{T}_1 > 0$, $\mathrm{T}_2 > 0$, $0 < \zeta < 1$, $\mathrm{M}_1 > 0$, $\mathrm{M}_2 > 0$ and $\mathrm{M}_3 > 0$ are positive given constants. The controller is triggered at time instant t_k with $k \in \mathrm{N}^*$. During the time interval $t \in \left[t_k, t_{k+1}\right)$, the value of actuator's input $\mu_{PFi}(t)$ holds unchanged as a constant, i.e., $\varpi_i\left(t_k\right)$. Every time when event is triggered, the time t will be marked as t_{k+1}.

For the improved STM, the following transformation is given

$$e_1 = \max\left\{\mathrm{M}_1, \mathrm{M}_2, \zeta \mathrm{T}_2 + \mathrm{M}_3\right\} \tag{6}$$

For system (4), the aims of proposed control scheme in this paper are three-folds: (i) all signals of the closed-loop system are bounded in probability; (ii) tracking error evolves within an arbitrarily small range around the origin; (iii) the controller excludes Zeno behavior.

In order to design a controller with outstanding performance to achieve the above control aims, the following Assumptions are given.

Assumption 1. The reference signal y_d and up to its nth order time derivatives are continuous and bounded.

Assumption 2. In system (1), $\varphi_i(\chi) \neq 0$, $c_i \neq 0$, and sign $\left(c_i\right)$ is known.

Assumption 3. To ensure the performance of the considered system, the maximum number of total failed actuators is $w - 1$, while the number of partial failed actuators can reach w.

Assume that w_j $\left(0 \leq w_j \leq w\right)$ actuator is failure and no new failures appear in the time interval $\left[T_j, T_{j+1}\right)$. The PLOE and failure-free actuator's set is Q_{PTj} in time interval $\left[T_j, T_{j+1}\right)$ and the TLOE actuator's set is Q_{TTj}. Therefore, it is obvious that $Q_{PTj} \cup Q_{TTj} \equiv \{1, 2, \ldots, w\}$.

Remark 2. Assumptions 1–3 are common in existing relevant literatures, see [27,33]. For example, many signals satisfy Assumption 1 with sinusoidal signals are typical examples in practice. Assumption 3 is fundamental to guarantee the controllability of the system (4) and the existence of a nominal solution to the adaptive failure compensation problem.

2.2. Stochastic system theory preparation

For the stochastic nonlinear system, its relevant theories will be given by the following general form

$$d\chi = G(\chi)\, dt + H(\chi)\, d\vartheta \tag{7}$$

where $\chi \in R^n$ denotes the system state, ϑ is expressed in system (1). The locally Lipschitz functions $G(\chi) \in R^n$ and $H(\chi) \in R^{n\times r}$ satisfy initial conditions $G(\mathbf{0}) = \mathbf{0}$ and $H(\mathbf{0}) = \mathbf{0}$.

Definition 1 ([33]). For any Lyapunov function $V(\chi)$, the system (7) with differential operator ℓ is defined as

$$\ell V = \frac{\partial V}{\partial \chi} G(\chi) + \frac{1}{2}\mathrm{Tr}\left\{H^{\mathrm{T}}(\chi)\frac{\partial^2 V}{\partial \chi^2} H(\chi)\right\} \tag{8}$$

Lemma 1 ([7]). *For $\chi \in R^n$ and $t > 0$, there exist function $\Psi(\chi) \in C^2$, two constants $a > 0$ and $b > 0$, κ_∞ functions $\Gamma_1(\cdot)$ and $\Gamma_2(\cdot)$, such that*

$$\begin{cases} \Gamma_1(\|\chi\|) \leq \Psi(\chi) \leq \Gamma_2(\|\chi\|) \\ \ell\Psi(\chi) \leq -a\Psi(\chi) + b \end{cases} \tag{9}$$

Then, the system (4) certainly has a unique solution and is bounded in probability.

Lemma 2 ([10]). *For any two real constants x and y, the following inequality holds*

$$xy \leq \frac{o^{\upsilon}}{\upsilon}|x|^{\upsilon} + \frac{1}{\tau o^{\tau}}|y|^{\tau} \tag{10}$$

where $o > 0$, $\upsilon > 1$, $\tau > 1$ and $(\upsilon - 1)(\tau - 1) = 1$.

2.3. Approximation method research

In this subsection, the unknown function is approximated via MTN. The structure of MTN is given in [11–13], and its approximation principle is shown in Lemma 3.

Lemma 3 ([30]). *On a compact set $\Omega_\sigma \in R^n$, if there exist an unknown function $\mathrm{P}(\boldsymbol{\sigma})$ and constant $\forall \xi > 0$, then an MTN can be able to approximate $\mathrm{P}(\boldsymbol{\sigma})$. The approximation rule is as follows:*

$$\mathrm{P}(\boldsymbol{\sigma}) = \boldsymbol{\varsigma}^{*T} S_{m_n}(\boldsymbol{\sigma}) + \delta(\boldsymbol{\sigma}), \quad |\delta(\boldsymbol{\sigma})| \leq \xi \tag{11}$$

where $\boldsymbol{\varsigma}^* = \left[\varsigma_1, \ldots, \varsigma_l\right]^T \in R^l$ denotes the optimal weight vector of MTN, which is defined as

$$\boldsymbol{\varsigma}^* := arg \min_{\varsigma \in R^l}\left\{\sup_{\sigma \in \Omega_\sigma}\left|\mathrm{P}(\boldsymbol{\sigma}) - \boldsymbol{\varsigma}^T S_{m_n}(\boldsymbol{\sigma})\right|\right\}.$$

$S_{m_n}(\boldsymbol{\sigma}) = \left[\sigma_1, \ldots, \sigma_n, \sigma_1^2, \sigma_1\sigma_2, \ldots, \sigma_n^2, \ldots, \sigma_1^m, \ldots, \sigma_n^m\right]^T \in R^l$ and $\boldsymbol{\sigma} = \left[\sigma_1, \ldots, \sigma_n\right]^T \in \Omega_\sigma$ are the middle layer vector and the input layer vector of MTN, respectively. $\delta(\boldsymbol{\sigma})$ represents the approximation error between $\mathrm{P}(\boldsymbol{\sigma})$ and $\boldsymbol{\varsigma}^{*T} S_{m_n}(\boldsymbol{\sigma})$, which can be reduce to arbitrarily small.

Remark 3. Although both MTN and NN have the three layer network structure consisting of input, intermediate and output layers in form, their main difference is the way of information processing in the intermediate layer. Specifically, the MTN uses a polynomial combination of inputs instead of the traditional intermediate layer of radial basis functions, which allows the approximation of nonlinear functions with less computational overhead. Therefore, the MTN-based controller has unique advantage in reducing the computational burden.

3. Main research results

The development of the improved STM-based adaptive FTC scheme is highlighted in this section, followed by a demonstration of the control aims achieved by the closed-loop system (4).

At first, we introduce the following coordinate transformation to implement the backstepping design process:

$$\begin{cases} \varrho_1 = \chi_1 - y_d \\ \varrho_j = \chi_j - \mathfrak{T}_{j-1},\ j = 2,3,\ldots,n \end{cases} \tag{12}$$

where $\mathfrak{T}_{j-1}$ is virtual control law, which will be designed in the next subsection.

In view of (4) and (12), we have

$$\begin{cases} d\varrho_1 = \left(\chi_2 + f_1 - \dot{y}_d\right) dt + \phi_1^{\mathrm{T}} d\vartheta \\ d\varrho_j = \left(\chi_{j+1} + f_j - \nabla\mathfrak{T}_{j-1}\right) dt + \bar{\phi}_j^{\mathrm{T}} d\vartheta \\ \quad j = 2,3,\ldots,n-1 \\ d\varrho_n = (\sum_{i=1}^{w} c_i \varphi_i(\chi)\left(\lambda_i \mu_{PFi}(t) + \mu_{TFi}\right) \\ \qquad + f_n + \Gamma(t)\mathrm{P}(\chi) - \nabla\mathfrak{T}_{n-1}) dt + \bar{\phi}_n^{\mathrm{T}} d\vartheta \end{cases} \tag{13}$$

where $\bar{\phi}_j = \phi_j - \sum_{i=1}^{j-1} \frac{\partial \mathfrak{T}_{j-1}}{\partial x_i} \phi_i$, and $\nabla\mathfrak{T}_{j-1}$ is the time partial derivative of $\mathfrak{T}_{j-1}$, which will be given in the next subsection.

The virtual adaptive law $\dot{\hat{\varsigma}}_j$ and the virtual control law $\mathfrak{T}_j$ are individually designed as follows

$$\dot{\hat{\varsigma}}_j = \varrho_j^3 S_{m_j} - \beta_j \hat{\varsigma}_j \tag{14}$$

$$\mathfrak{T}_j = -r_j \varrho_j - \hat{\varsigma}_j^{\mathrm{T}} S_{m_j} \tag{15}$$

where $1 \le j \le n-1$, r_j and β_j are positive constants, and $\hat{\varsigma}_j$ will be defined later.

3.1. Event-triggered adaptive controller design

Step 1: Constructing the Lyapunov function Ψ_1 as

$$\Psi_1 = \frac{1}{4}\varrho_1^4 + \frac{1}{2}\tilde{\varsigma}_1^{\mathrm{T}}\tilde{\varsigma}_1 \tag{16}$$

where $\tilde{\varsigma}_1 = \varsigma_1 - \hat{\varsigma}_1$ is the first error vector, and $\hat{\varsigma}_1$ denotes the estimation error of ς_1.

Based on Definition 1, and according to (13) and (16), we obtain

$$\ell\Psi_1 = \varrho_1^3\left(\chi_2 + f_1 - \dot{y}_d\right) + \frac{3}{2}\varrho_1^2\phi_1^{\mathrm{T}}\phi_1 - \tilde{\varsigma}_1^{\mathrm{T}}\dot{\hat{\varsigma}}_1 \tag{17}$$

By utilizing Lemma 2, the following inequality holds

$$\frac{3}{2}\varrho_1^2\phi_1^{\mathrm{T}}\phi_1 \le \frac{3}{4\gamma_1^2}\varrho_1^4\|\phi_1\|^4 + \frac{3}{4}\gamma_1^2 \tag{18}$$

where $\gamma_1 > 0$ is a constant.

Substituting (18) into (17), and simply transforming yields

$$\ell\Psi_1 \le \varrho_1^3\left(\varrho_2 + \mathfrak{T}_1 + F_1\right) - \frac{3}{2}\varrho_1^4 + \frac{3}{4}\gamma_1^2 - \tilde{\varsigma}_1^{\mathrm{T}}\dot{\hat{\varsigma}}_1 \tag{19}$$

where $F_1 = f_1 - \dot{y}_d + \frac{3}{2}\varrho_1 + \frac{3}{4\gamma_1^2}\varrho_1\|\phi_1\|^4$.

The unknown nonlinear function F_1 in (19) cannot be applied directly to the controller design. Therefore, by utilizing Lemma 3, for $\forall\xi_1 > 0$, an MTN $\varsigma_1^{\mathrm{T}} S_{m_1}(Z_1)$ can be employed to approximate it in the following form:

$$F_1 = \varsigma_1^{\mathrm{T}} S_{m_1}(Z_1) + \delta_1(Z_1) \tag{20}$$

where $Z_1 = [\varrho_1]^{\mathrm{T}}$, and $\delta_1(Z_1)$ denotes the error between $\varsigma_1^{\mathrm{T}} S_{m_1}(Z_1)$ and $F_1(Z_1)$, and satisfying $\left|\delta_1(Z_1)\right| \le \xi_1$.

Furthermore, the following inequality can be obtained by utilizing Lemma 2:

$$\varrho_1^3\left(\varrho_2 + \delta_1\right) \le \frac{1}{4}\varrho_2^4 + \frac{3}{2}\varrho_1^4 + \frac{1}{4}\xi_1^4 \tag{21}$$

By combining (14), (15), (20) and (21), the (19) can be expressed as

$$\ell\Psi_1 \le -r_1\varrho_1^4 + \frac{3}{4}\gamma_1^2 + \frac{1}{4}\xi_1^4 + \beta_1\tilde{\varsigma}_1^{\mathrm{T}}\hat{\varsigma}_1 + \frac{1}{4}\varrho_2^4 \tag{22}$$

Step j $(2 \le j \le n-1)$: Constructing the Lyapunov function Ψ_j as

$$\Psi_j = \Psi_{j-1} + \frac{1}{4}\varrho_j^4 + \frac{1}{2}\tilde{\varsigma}_j^{\mathrm{T}}\tilde{\varsigma}_j \tag{23}$$

where $\tilde{\varsigma}_j = \varsigma_j - \hat{\varsigma}_j$ is jth error vector, and $\hat{\varsigma}_j$ denotes the estimation error of ς_j.

Based on Definition 1, and according to (13) and (23), we obtain

$$\begin{aligned} \ell\Psi_j = {} & \ell\Psi_{j-1} + \varrho_j^3\left(\chi_{j+1} + f_j - \nabla\mathfrak{T}_{j-1}\right) \\ & + \frac{3}{2}\varrho_j^2\bar{\phi}_j^{\mathrm{T}}\bar{\phi}_j - \tilde{\varsigma}_j^{\mathrm{T}}\dot{\hat{\varsigma}}_j \end{aligned} \tag{24}$$

where $\nabla\mathfrak{T}_{j-1} = \sum_{i=1}^{j-1}\frac{\partial\mathfrak{T}_{j-1}}{\partial\chi_i}\left(\chi_{i+1} + f_i\right) + \frac{1}{2}\sum_{p,q=1}^{j-1}\frac{\partial^2\mathfrak{T}_{j-1}}{\partial\chi_p\partial\chi_q}\phi_p^{\mathrm{T}}\phi_q + \sum_{i=0}^{j-1}\frac{\partial\mathfrak{T}_{j-1}}{\partial y_d^{(i)}} y_d^{(i+1)} + \sum_{i=1}^{j-1}\frac{\partial\mathfrak{T}_{j-1}}{\hat{\varsigma}_i}\dot{\hat{\varsigma}}_i$.

By utilizing Lemma 2, the following inequality holds

$$\frac{3}{2}\varrho_j^2\bar{\phi}_j^{\mathrm{T}}\bar{\phi}_j \le \frac{3}{4\gamma_j^2}\varrho_j^4\left\|\bar{\phi}_j\right\|^4 + \frac{3}{4}\gamma_j^2 \tag{25}$$

where $\gamma_j > 0$ is a constant.

Substituting (25) into (24), and simply transforming yields

$$\begin{aligned} \ell\Psi_j \le {} & \ell\Psi_{j-1} + \varrho_j^3\left(\varrho_{j+1} + \mathfrak{T}_j + F_j\right) \\ & - \frac{7}{4}\varrho_j^4 + \frac{3}{4}\gamma_j^2 - \tilde{\varsigma}_j^{\mathrm{T}}\dot{\hat{\varsigma}}_j \end{aligned} \tag{26}$$

where $F_j = f_j - \nabla\mathfrak{T}_{j-1} + \frac{7}{4}\varrho_j + \frac{3}{4\gamma_j^2}\varrho_j\left\|\bar{\phi}_j\right\|^4$.

Similarly, by utilizing Lemma 3, for $\forall\xi_j > 0$, an MTN $\varsigma_j^{\mathrm{T}} S_{m_j}(Z_j)$ can be employed to approximate F_j:

$$F_j = \varsigma_j^{\mathrm{T}} S_{m_j}(Z_j) + \delta_j(Z_j) \tag{27}$$

where $Z_j = [\varrho_1, \varrho_2, \ldots, \varrho_j]^{\mathrm{T}}$, and $\delta_j(Z_j)$ denotes the error between $\varsigma_j^{\mathrm{T}} S_{m_j}(Z_j)$ and $F_j(Z_j)$, and satisfying $\left|\delta_j(Z_j)\right| \le \xi_j$.

Furthermore, the following inequality can be obtained by utilizing Lemma 2.

$$\varrho_j^3\left(\varrho_{j+1} + \delta_j\right) \le \frac{1}{4}\varrho_{j+1}^4 + \frac{3}{2}\varrho_j^4 + \frac{1}{4}\xi_j^4 \tag{28}$$

By combining (14), (15), (27) and (28), the (26) can be expressed as

$$\begin{aligned} \ell\Psi_j \le {} & -\sum_{i=1}^{j} r_i\varrho_i^4 + \frac{3}{4}\sum_{i=1}^{j}\gamma_i^2 + \sum_{i=1}^{j}\beta_i\tilde{\varsigma}_i^{\mathrm{T}}\hat{\varsigma}_i \\ & + \frac{1}{4}\sum_{i=1}^{j}\xi_i^4 + \frac{1}{4}\varrho_{j+1}^4 \end{aligned} \tag{29}$$

Step n: During the time interval $[T_j, T_{j+1})$, we construct the following Lyapunov function Ψ_n as

$$\begin{aligned} \Psi_n = {} & \Psi_{n-1} + \frac{1}{4}\varrho_n^4 + \frac{1}{2}\tilde{\varsigma}_n^{\mathrm{T}}\tilde{\varsigma}_n + \frac{1}{2}\tilde{\boldsymbol{v}}^{\mathrm{T}}\tilde{\boldsymbol{v}} \\ & + \frac{1}{2}\sum_{\substack{i=1, \\ i\in\mathcal{Q}_{PTj}}}^{w} |c_i|\,\lambda_i\tilde{\boldsymbol{k}}^{\mathrm{T}}\tilde{\boldsymbol{k}} \end{aligned} \tag{30}$$

where $\tilde{\varsigma}_n = \varsigma_n - \hat{\varsigma}_n$ is nth error vector, and $\hat{\varsigma}_n$ denotes the estimation error of ς_n, similarly, $\tilde{\boldsymbol{v}} = \boldsymbol{v} - \hat{\boldsymbol{v}}$ and $\tilde{\boldsymbol{k}} = \boldsymbol{k}_j - \hat{\boldsymbol{k}}$ with $\boldsymbol{k}_j$ and $\hat{\boldsymbol{k}}$ will be defined later.

Based on Definition 1, and according to (13) and (30), we obtain

$$\begin{aligned} \ell\Psi_n = {} & \ell\Psi_{n-1} + \varrho_n^3\sum_{i=1}^{w} c_i\varphi_i(\chi)\left(\mu_{TFi} + \lambda_i\mu_{PFi}(t)\right) \\ & + \varrho_n^3\left(f_n + \Gamma(t)\mathrm{P}(\chi) - \nabla\mathfrak{T}_{n-1}\right) + \frac{3}{2}\varrho_n^2\bar{\phi}_n^{\mathrm{T}}\bar{\phi}_n \\ & - \tilde{\varsigma}_n^{\mathrm{T}}\dot{\hat{\varsigma}}_n - \tilde{\boldsymbol{v}}^{\mathrm{T}}\dot{\hat{\boldsymbol{v}}} - \sum_{\substack{i=1, \\ i\in\mathcal{Q}_{PTj}}}^{w} |c_i|\,\lambda_i\tilde{\boldsymbol{k}}^{\mathrm{T}}\dot{\hat{\boldsymbol{k}}} \end{aligned} \tag{31}$$

where $\nabla\mathfrak{F}_{n-1} = \sum_{i=1}^{n-1}\frac{\partial\mathfrak{F}_{n-1}}{\partial\chi_i}\left(\chi_{i+1}+f_i\right) + \frac{1}{2}\sum_{p,q=1}^{n-1}\frac{\partial^2\mathfrak{F}_{n-1}}{\partial\chi_p\partial\chi_q}\phi_p^{\mathrm{T}}\phi_q + \sum_{i=0}^{n-1}\frac{\partial\mathfrak{F}_{n-1}}{\partial y_d^{(i)}}y_d^{(i+1)} + \sum_{i=1}^{n-1}\frac{\partial\mathfrak{F}_{n-1}}{\hat{\varsigma}_i}\dot{\hat{\varsigma}}_i$.

By utilizing Lemma 2, the following inequality holds

$$\frac{3}{2}\varrho_n^2\bar{\phi}_n^{\mathrm{T}}\bar{\phi}_n \le \frac{3}{4\gamma_n^2}\varrho_n^4\left\|\bar{\phi}_n\right\|^4 + \frac{3}{4}\gamma_n^2 \tag{32}$$

where $\gamma_n > 0$ is a constant.

Substituting (32) into (31), and simply transforming yields

$$\begin{aligned}\ell\Psi_n \le{}& \ell\Psi_{n-1} + \varrho_n^3\sum_{i=1}^{w}c_i\varphi_i(\chi)\left(\mu_{TFi}+\lambda_i\mu_{PFi}(t)\right)\\ &+ \varrho_n^3\left(\Gamma(t)\mathrm{P}(\chi)+F_n\right) - \frac{7}{4}\varrho_n^4 + \frac{3}{4}\gamma_n^2\\ &- \tilde{\varsigma}_n^{\mathrm{T}}\dot{\hat{\varsigma}}_n - \tilde{\boldsymbol{v}}^{\mathrm{T}}\dot{\hat{\boldsymbol{v}}} - \sum_{\substack{i=1,\\ i\in Q_{PTj}}}^{w}|c_i|\lambda_i\tilde{\boldsymbol{k}}^{\mathrm{T}}\dot{\hat{\boldsymbol{k}}}\end{aligned} \tag{33}$$

where $F_n = f_n - \nabla\mathfrak{F}_{n-1} + \frac{7}{4}\varrho_n + \frac{3}{4\gamma_n^2}\varrho_n\left\|\bar{\phi}_n\right\|^4$.

Similarly, by utilizing Lemma 3, for $\forall\xi_n > 0$, an MTN $\varsigma_n^{\mathrm{T}}S_{m_n}(\boldsymbol{Z}_n)$ can be employed to approximate F_n:

$$F_n = \varsigma_n^{\mathrm{T}}S_{m_n}(\boldsymbol{Z}_n) + \delta_n(\boldsymbol{Z}_n) \tag{34}$$

where $\boldsymbol{Z}_n = [\varrho_1, \varrho_2, \ldots, \varrho_n]^{\mathrm{T}}$, and $\delta_n(\boldsymbol{Z}_n)$ is the error of $\varsigma_n^{\mathrm{T}}S_{m_n}(\boldsymbol{Z}_n)$ and $F_n(\boldsymbol{Z}_n)$, and satisfying $\left|\delta_n(\boldsymbol{Z}_n)\right| \le \xi_n$.

Furthermore, by utilizing Lemma 3, for $\forall\xi > 0$, the system external failure $\mathrm{P}(\chi)$ as an unknown function which can be approximated by employing an MTN $\boldsymbol{v}^{\mathrm{T}}\bar{S}_{m_n}(\chi)$.

$$\mathrm{P}(\chi) = \boldsymbol{v}^{\mathrm{T}}\bar{S}_{m_n}(\chi) + \delta(\chi) \tag{35}$$

where $\chi = [\chi_1, \chi_2, \ldots, \chi_n]^{\mathrm{T}}$, and $\delta(\chi)$ denotes the error between $\boldsymbol{v}^{\mathrm{T}}\bar{S}_{m_n}(\chi)$ and $\mathrm{P}(\chi)$, and satisfying $|\delta(\chi)| \le \xi$.

Then, the following inequalities can be obtained by utilizing Lemma 2.

$$\varrho_n^3F_n \le \varrho_n^3\varsigma_n^{\mathrm{T}}S_{m_n}(\boldsymbol{Z}_n) + \frac{1}{4}\xi_n^4 + \frac{3}{4}\varrho_n^4 \tag{36}$$

$$\varrho_n^3\Gamma(t)\mathrm{P}(\chi) \le \varrho_n^3\boldsymbol{v}^{\mathrm{T}}\bar{S}_{m_n}(\chi) + \frac{1}{4}\xi^4 + \frac{3}{4}\varrho_n^4 \tag{37}$$

By combining (36) and (37), the (33) can be expressed as

$$\begin{aligned}\ell\Psi_n \le{}& \ell\Psi_{n-1} + \varrho_n^3\sum_{i=1}^{w}c_i\varphi_i(\chi)\left(\mu_{TFi}+\lambda_i\mu_{PFi}(t)\right)\\ &+ \varrho_n^3\left(\varsigma_n^{\mathrm{T}}S_{m_n} + \boldsymbol{v}^{\mathrm{T}}\bar{S}_{m_n}\right) - \sum_{\substack{i=1,\\ i\in Q_{PTj}}}^{w}|c_i|\lambda_i\tilde{\boldsymbol{k}}^{\mathrm{T}}\dot{\hat{\boldsymbol{k}}}\\ &- \frac{1}{4}\varrho_n^4 + \frac{3}{4}\gamma_n^2 + \frac{1}{4}\xi_n^4 + \frac{1}{4}\xi^4 - \tilde{\varsigma}_n^{\mathrm{T}}\dot{\hat{\varsigma}}_n - \tilde{\boldsymbol{v}}^{\mathrm{T}}\dot{\hat{\boldsymbol{v}}}\end{aligned} \tag{38}$$

Based on (38), the event-triggered controller $\varpi_i(t)$, and the adaptive laws $\dot{\hat{\varsigma}}_n$, $\dot{\hat{\boldsymbol{v}}}$ are given as

$$\varpi_i(t) = \bar{\mu}_{bi} - \bar{\mathrm{M}}\tanh\left(\frac{\Theta_i}{\eta}\right) \tag{39}$$

$$\dot{\hat{\varsigma}}_n = \varrho_n^3S_{m_n} - \beta_n\hat{\varsigma}_n \tag{40}$$

$$\dot{\hat{\boldsymbol{v}}} = \varrho_n^3\bar{S}_{m_n} - \beta\hat{\boldsymbol{v}} \tag{41}$$

with $\Theta_i = \varrho_n^3\operatorname{sign}(c_i)\varphi_i(\chi)\bar{\mathrm{M}}$, where $\bar{\mathrm{M}} \ge e_1$, $\beta_n > 0$ and $\beta > 0$ are constants.

From (5) and (6), we can get $\mu_{PFi}(t) = \varpi_i(t) - h(t)e_1$ where $h(t)$ is a time-varying parameter satisfying $|h(t)| \le 1$.

Furthermore, see in [17], the function $\tanh(\cdot)$ has the following property as follows:

$$0 \le |\boldsymbol{\Phi}| - \boldsymbol{\Phi}\tanh\left(\frac{\boldsymbol{\Phi}}{\eta}\right) \le 0.2785\eta \tag{42}$$

where $\boldsymbol{\Phi} \in R$ and $\eta > 0$.

Then, substituting $\mu_{PFi}(t) = \varpi_i(t) - h(t)e_1$ into $\varrho_n^3\operatorname{sign}(c_i)\varphi_i(\chi)\mu_{PFi}(t)$ yields

$$\begin{aligned}&\varrho_n^3\operatorname{sign}(c_i)\varphi_i(\chi)\mu_{PFi}(t)\\ ={}&\varrho_n^3\operatorname{sign}(c_i)\varphi_i(\chi)\left(\varpi_i(t) - h(t)e_1\right)\\ ={}&\varrho_n^3\operatorname{sign}(c_i)\varphi_i(\chi)\bar{\mu}_{bi}\\ &- \varrho_n^3\operatorname{sign}(c_i)\varphi_i(\chi)h(t)e_1\\ &- \varrho_n^3\operatorname{sign}(c_i)\varphi_i(\chi)\bar{\mathrm{M}}\tanh\left(\frac{\Theta_i}{\eta}\right)\\ \le{}&\varrho_n^3\operatorname{sign}(c_i)\varphi_i(\chi)\bar{\mu}_{bi} - |\Theta_i| + 0.2785\eta\\ &- \varrho_n^3\operatorname{sign}(c_i)\varphi_i(\chi)h(t)e_1\\ \le{}&\varrho_n^3\operatorname{sign}(c_i)\varphi_i(\chi)\bar{\mu}_{bi} + 0.2785\eta\end{aligned} \tag{43}$$

By combining (40), (41) and (43), the (38) can be rewritten as

$$\begin{aligned}\ell\Psi_n \le{}& \ell\Psi_{n-1} + \varrho_n^3\sum_{i=1}^{w}c_i\varphi_i(\chi)\left(\mu_{TFi}+\lambda_i\bar{\mu}_{bi}\right)\\ &+ \varrho_n^3\left(\hat{\varsigma}_n^{\mathrm{T}}S_{m_n} + \hat{\boldsymbol{v}}^{\mathrm{T}}\bar{S}_{m_n}\right) - \sum_{\substack{i=1,\\ i\in Q_{PTj}}}^{w}|c_i|\lambda_i\tilde{\boldsymbol{k}}^{\mathrm{T}}\dot{\hat{\boldsymbol{k}}}\\ &- \frac{1}{4}\varrho_n^4 + \frac{3}{4}\gamma_n^2 + \frac{1}{4}\xi_n^4 + \frac{1}{4}\xi^4 + \beta_n\tilde{\varsigma}_n^{\mathrm{T}}\hat{\varsigma}_n\\ &+ \beta\tilde{\boldsymbol{v}}^{\mathrm{T}}\hat{\boldsymbol{v}} + 0.2785\eta\sum_{i=1}^{w}\lambda_i|c_i|\end{aligned} \tag{44}$$

Based on (44), we design the actual control law $\bar{\mu}_{bi}$ as

$$\bar{\mu}_{bi} = \operatorname{sign}(c_i)\frac{1}{\varphi_i(\chi)}\boldsymbol{k}_j^{\mathrm{T}}\boldsymbol{\omega},\ i = 1, 2, \ldots, w \tag{45}$$

where $\boldsymbol{\omega} = (\omega_1, \varphi_1, \ldots, \varphi_w)^{\mathrm{T}}$, $\boldsymbol{k}_j = (k_{j,1}, k_{j,21}, \ldots, k_{j,2w})^{\mathrm{T}}$.

The following formula holds in the time interval $[T_j, T_{j+1})$.

$$\sum_{\substack{i=1,\\ i\in Q_{PTj}}}^{w}|c_i|\lambda_i\boldsymbol{k}_j^{\mathrm{T}}\boldsymbol{\omega} = \mathfrak{F}_n - \sum_{\substack{i=1,\\ i\in Q_{TTj}}}^{w}c_i\varphi_i(\chi)\mu_{TFi} \tag{46}$$

where $\boldsymbol{k}_j$ and $\boldsymbol{\omega}$ are defined as

$$\begin{cases}k_{j,1} = \dfrac{1}{\sum_{\substack{i=1,\\ i\in Q_{PTj}}}^{w}|c_i|\lambda_i}, k_{j,2i} = \dfrac{-c_i\mu_{TFi}}{\sum_{\substack{i=1,\\ i\in Q_{PTj}}}^{w}|c_i|\lambda_i},\\ \text{for } i \in Q_{TTj},\ k_{j,2i} = 0,\ \text{for } i \in Q_{PTj};\\ \omega_1 = \mathfrak{F}_n\end{cases} \tag{47}$$

Due to the existence of uncertain actuator failure model and unknown parameters, $\boldsymbol{k}_j$ needs to be estimated. Therefore, the actual control law $\bar{\mu}_{bi}$ can be rewritten as

$$\bar{\mu}_{bi} = \operatorname{sign}(c_i)\frac{1}{\varphi_i(\chi)}\hat{\boldsymbol{k}}^{\mathrm{T}}\boldsymbol{\omega},\ i = 1, 2, \ldots, w \tag{48}$$

where $\hat{\boldsymbol{k}}$ denotes the estimate of $\boldsymbol{k}_j$.

According to $\tilde{\boldsymbol{k}} = \boldsymbol{k}_j - \hat{\boldsymbol{k}}$, (46) and (48), we can deduce that

$$\begin{aligned}&\varrho_n^3\sum_{i=1}^{w}c_i\varphi_i(\chi)\left(\mu_{TFi}+\lambda_i\bar{\mu}_{bi}\right) - \sum_{\substack{i=1,\\ i\in Q_{PTj}}}^{w}|c_i|\lambda_i\tilde{\boldsymbol{k}}^{\mathrm{T}}\dot{\hat{\boldsymbol{k}}}\\ ={}&\varrho_n^3\sum_{\substack{i=1,\\ i\in Q_{PTj}}}^{w}|c_i|\lambda_i\hat{\boldsymbol{k}}^{\mathrm{T}}\boldsymbol{\omega} - \sum_{\substack{i=1,\\ i\in Q_{PTj}}}^{w}|c_i|\lambda_i\tilde{\boldsymbol{k}}^{\mathrm{T}}\dot{\hat{\boldsymbol{k}}}\\ &+ \varrho_n^3\left(\mathfrak{F}_n - \sum_{\substack{i=1,\\ i\in Q_{PTj}}}^{w}|c_i|\lambda_i\boldsymbol{k}_j^{\mathrm{T}}\boldsymbol{\omega}\right)\\ ={}&\varrho_n^3\mathfrak{F}_n - \varrho_n^3\sum_{\substack{i=1,\\ i\in Q_{PTj}}}^{w}|c_i|\lambda_i\tilde{\boldsymbol{k}}^{\mathrm{T}}\boldsymbol{\omega} - \sum_{\substack{i=1,\\ i\in Q_{PTj}}}^{w}|c_i|\lambda_i\tilde{\boldsymbol{k}}^{\mathrm{T}}\dot{\hat{\boldsymbol{k}}}\\ ={}&\varrho_n^3\mathfrak{F}_n - \sum_{\substack{i=1,\\ i\in Q_{PTj}}}^{w}|c_i|\lambda_i\tilde{\boldsymbol{k}}^{\mathrm{T}}\left(\dot{\hat{\boldsymbol{k}}} + \varrho_n^3\boldsymbol{\omega}\right)\end{aligned} \tag{49}$$

Then, substituting (49) into (44) yields

$$\begin{aligned}\mathscr{L}\Psi_n \le{}& \mathscr{L}\Psi_{n-1} + \varrho_n^3\left(\mathfrak{F}_n + \hat{\varsigma}_n^{\mathrm{T}} S_{m_n} + \hat{\boldsymbol{\upsilon}}^{\mathrm{T}}\bar{S}_{m_n}\right)\\ &- \frac{1}{4}\varrho_n^4 + \frac{3}{4}\gamma_n^2 + \frac{1}{4}\xi_n^4 + \frac{1}{4}\xi^4 + \beta_n\tilde{\varsigma}_n^{\mathrm{T}}\hat{\varsigma}_n\\ &+ \beta\tilde{\boldsymbol{\upsilon}}^{\mathrm{T}}\hat{\boldsymbol{\upsilon}} + 0.2785\eta\sum_{i=1}^{w}\lambda_i|c_i|\\ &- \sum_{\substack{i=1,\\ i\in Q_{PTj}}}^{w}|c_i|\lambda_i\tilde{\boldsymbol{k}}^{\mathrm{T}}\left(\dot{\hat{\boldsymbol{k}}} + \varrho_n^3\boldsymbol{\omega}\right)\end{aligned} \tag{50}$$

Based on (50), the update law $\dot{\hat{\boldsymbol{k}}}$ and the virtual control law $\mathfrak{F}_n$ are designed as

$$\dot{\hat{\boldsymbol{k}}} = \varrho_n^3\boldsymbol{\omega} - \beta_k\hat{\boldsymbol{k}} \tag{51}$$

$$\mathfrak{F}_n = -r_n\varrho_n - \hat{\varsigma}_n^{\mathrm{T}}S_{m_n} - \hat{\boldsymbol{\upsilon}}^{\mathrm{T}}\bar{S}_{m_n} \tag{52}$$

where $\beta_k > 0$ and $r_n > 0$ are constants.

By combining (29), (51) and (52), the (50) can be expressed as

$$\begin{aligned}\mathscr{L}\Psi_n \le{}& \sum_{i=1}^{n}\left(-r_i\varrho_i^4 + \frac{3}{4}\gamma_i^2 + \frac{1}{4}\xi_i^4 + \beta_i\tilde{\varsigma}_i^{\mathrm{T}}\hat{\varsigma}_i\right)\\ &+ \frac{1}{4}\xi^4 + \beta\tilde{\boldsymbol{\upsilon}}^{\mathrm{T}}\hat{\boldsymbol{\upsilon}} + 0.2785\eta\sum_{i=1}^{w}\lambda_i|c_i|\\ &+ \sum_{\substack{i=1,\\ i\in Q_{PTj}}}^{w}|c_i|\lambda_i\beta_k\tilde{\boldsymbol{k}}^{\mathrm{T}}\hat{\boldsymbol{k}}\end{aligned} \tag{53}$$

Then, by utilizing Lemma 2, the following inequality can be obtained.

$$\begin{aligned}\beta_i\tilde{\varsigma}_i^{T}\hat{\varsigma}_i &= \beta_i\tilde{\varsigma}_i^{T}\left(\varsigma_i - \tilde{\varsigma}_i\right) = \beta_i\tilde{\varsigma}_i^{T}\varsigma_i - \beta_i\tilde{\varsigma}_i^{T}\tilde{\varsigma}_i\\ &\leqslant \frac{\beta_i}{2}\tilde{\varsigma}_i^{T}\tilde{\varsigma}_i + \frac{\beta_i}{2}\left\|\varsigma_i\right\|^2 - \beta_i\tilde{\varsigma}_i^{T}\tilde{\varsigma}_i\\ &= -\frac{\beta_i}{2}\tilde{\varsigma}_i^{T}\tilde{\varsigma}_i + \frac{\beta_i}{2}\left\|\varsigma_i\right\|^2\end{aligned} \tag{54}$$

Similar to the derivation process of (54), we can further obtain

$$\beta\tilde{\boldsymbol{\upsilon}}^{\mathrm{T}}\hat{\boldsymbol{\upsilon}} \le -\frac{\beta}{2}\tilde{\boldsymbol{\upsilon}}^{\mathrm{T}}\tilde{\boldsymbol{\upsilon}} + \frac{\beta}{2}\|\boldsymbol{\upsilon}\|^2 \tag{55}$$

$$\beta_k\tilde{\boldsymbol{k}}^{\mathrm{T}}\hat{\boldsymbol{k}} \le -\frac{\beta_k}{2}\tilde{\boldsymbol{k}}^{\mathrm{T}}\tilde{\boldsymbol{k}} + \frac{\beta_k}{2}\left\|\boldsymbol{k}_j\right\|^2 \tag{56}$$

Therefore, in view of (54), (55) and (56), the inequality (53) can be rewritten as

$$\begin{aligned}\mathscr{L}\Psi_n \le{}& -\sum_{i=1}^{n}\left(r_i\varrho_i^4 + \frac{\beta_i}{2}\tilde{\varsigma}_i^{\mathrm{T}}\tilde{\varsigma}_i\right) - \frac{\beta}{2}\tilde{\boldsymbol{\upsilon}}^{\mathrm{T}}\tilde{\boldsymbol{\upsilon}}\\ &- \sum_{\substack{i=1,\\ i\in Q_{PTj}}}^{w}\frac{|c_i|\lambda_i\beta_k}{2}\tilde{\boldsymbol{k}}^{\mathrm{T}}\tilde{\boldsymbol{k}} + \sum_{i=1}^{n}l_i\end{aligned} \tag{57}$$

where $l_i = \frac{3}{4}\gamma_i^2 + \frac{1}{4}\xi_i^4 + \frac{\beta_i}{2}\left\|\varsigma_i\right\|^2$, $i = 1, 2, \ldots, n-1$, $l_n = \frac{3}{4}\gamma_n^2 + \frac{1}{4}\xi_n^4 + \frac{1}{4}\xi^4 + \frac{\beta_n}{2}\left\|\varsigma_n\right\|^2 + \frac{\beta}{2}\|\boldsymbol{\upsilon}\|^2 + \frac{\beta_k}{2}\left\|\boldsymbol{k}_j\right\|^2 + 0.2785\eta\sum_{i=1}^{w}\lambda_i|c_i|$.

3.2. System stability analysis

Theorem 1. *The considered stochastic nonlinear system (4) is suffering from abrupt system external failure and uncertain actuator failures. Under Assumptions 1–3, the proposed control scheme, including the event-triggered controller (39), the ETM (5), the virtual control laws (15), (52), the actual control law (48), and the adaptive laws (14), (40), (41), (51). Then, one can verify that the following three aims hold as for any bounded initial condition.*

(1) All signals of the closed-loop system are bounded in probability.

(2) The tracking error evolves within an arbitrarily small range around the origin.

(3) The controller excludes Zeno behavior.

Proof. Based on the analysis in the previous section, the following Lyapunov function can be constructed for the n-order system (4)

$$\begin{aligned}V = {}& \frac{1}{4}\sum_{j=1}^{n}\varrho_j^4 + \frac{1}{2}\sum_{j=1}^{n}\tilde{\varsigma}_j^{\mathrm{T}}\tilde{\varsigma}_j + \frac{1}{2}\tilde{\boldsymbol{\upsilon}}^{\mathrm{T}}\tilde{\boldsymbol{\upsilon}}\\ &+ \sum_{\substack{i=1,\\ i\in Q_{PTj}}}^{w}\frac{|c_i|\lambda_i}{2}\tilde{\boldsymbol{k}}^{\mathrm{T}}\tilde{\boldsymbol{k}}\end{aligned} \tag{58}$$

According to (57), the following inequality holds

$$\begin{aligned}\mathscr{L}V \le{}& -\sum_{j=1}^{n}\left(r_j\varrho_j^4 + \frac{\beta_j}{2}\tilde{\varsigma}_j^{\mathrm{T}}\tilde{\varsigma}_j\right) - \frac{\beta}{2}\tilde{\boldsymbol{\upsilon}}^{\mathrm{T}}\tilde{\boldsymbol{\upsilon}}\\ &- \sum_{\substack{i=1,\\ i\in Q_{PTj}}}^{w}\frac{|c_i|\lambda_i\beta_k}{2}\tilde{\boldsymbol{k}}^{\mathrm{T}}\tilde{\boldsymbol{k}} + \sum_{j=1}^{n}l_j\end{aligned} \tag{59}$$

Let $a = \min\left\{4r_j, \beta_j\,(j = 1, 2, \ldots, n), \beta, \beta_k\right\}$ and $b = \sum_{j=1}^{n}l_j$, yields

$$\mathscr{L}V \le -aV + b,\ t \ge 0 \tag{60}$$

Firstly, according to Lemma 1 and (60), we get that ϱ_j, $\tilde{\varsigma}_j$, $\tilde{\boldsymbol{\upsilon}}$ and $\tilde{\boldsymbol{k}}$ are bounded in probability. Since ς_j, $\boldsymbol{\upsilon}$ and $\boldsymbol{k}$ are constants, we can infer that $\hat{\varsigma}_j$, $\hat{\boldsymbol{\upsilon}}$ and $\hat{\boldsymbol{k}}$ are bounded in probability. Therefore, $\mathfrak{F}_j$ composed of bounded signals ϱ_j, $\hat{\varsigma}_j$, $\hat{\boldsymbol{\upsilon}}$ and $\hat{\boldsymbol{k}}$, thus $\mathfrak{F}_j$ is also bounded in probability. By recalling $\varrho_j = \chi_j - \mathfrak{F}_{j-1}$, χ_j is also bounded in probability. Finally, we can further infer that the actual control law $\bar{\mu}_{bi}$ and event-triggered controller $\varpi_i(t)$ are also bounded in probability.

Secondly, according to (60) and [34] (Th. 4.1), we can obtain the following inequality

$$E\left[V(t)\right] \leqslant V(0)e^{-at} + \frac{b}{a} \tag{61}$$

which means that $\frac{1}{4}\varrho_j^4 \leqslant V(0)e^{-at} + \frac{b}{a}, \forall t > 0$. Next, one can further obtain

$$\lim_{t\to\infty}|\varrho_1| = \lim_{t\to\infty}|\chi_1 - y_d| \leqslant \sqrt[4]{\frac{4b}{a}} \tag{62}$$

Based on (62), by increasing l_j and reducing $4r_j$, β_j, β, β_k, the tracking error ϱ_1 can converge to an arbitrarily small range around the origin. Thereby, the control aims (1) and (2) can be realized.

Finally, we will demonstrate that the controller excludes Zeno behavior. There exists a constant $t^* > 0$ such that $\left\{t_{k+1} - t_k\right\} \geqslant t^*$, for $\forall k \in \mathrm{N}^*$. Then, by recalling $e(t) = \varpi_i(t) - \mu_{PFi}(t), \forall t \in \left[t_k, t_{k+1}\right)$, we can deduce

$$\frac{de(t)}{dt} \leqslant |\dot{e}(t)| = \left|\dot{\varpi}(t) - \dot{\mu}_{PFi}(t)\right| = |\dot{\varpi}(t)| \tag{63}$$

From (39), we can know that $\dot{\varpi}(t)$ is composed of bounded signals $\bar{\mu}_{bi}$, z_n and known smooth nonlinear function $\varphi_i(\chi)$, thus, there exists a constant $l > 0$ such that $|\dot{\varpi}(t)| \leqslant l$. In addition, through $e\left(t_k\right) = 0$ and $\lim_{t\to t_{k+1}}e(t) = \mathrm{M}_1$ or $\lim_{t\to t_{k+1}}e(t) = \mathrm{M}_2$ or $\lim_{t\to t_{k+1}}e(t) = \zeta\left|\mu_{PFi}(t)\right| + \mathrm{M}_3$, we can get that the lower bound of execution intervals t^* satisfy $t^* \geqslant \frac{\mathrm{M}_1}{l}$ or $t^* \geqslant \frac{\mathrm{M}_2}{l}$ or $t^* \geqslant \frac{\zeta|\mu_{PFi}(t)| + \mathrm{M}_3}{l} \geqslant \frac{\mathrm{M}_3}{l}$, which implies the Zeno behavior is effectively excluded.

Completing the proof of Theorem 1.

Remark 4. It is worth pointing out that when the amplitude of controller $\varpi_i(t)$ is large, or when the over-rate of change of the controller $\varpi_i(t)$ caused by other factors and two types of failures, if the controller is triggered, inevitably, a large signal impulse will act on the system, which will bring security hazards, so the FTM is used to provide

bounded error to overcome such situation. Conversely, when the amplitude of controller $\varpi_i(t)$ or the rate of change of the controller $\varpi_i(t)$ is small, switching to RTM to improve control performance. Therefore, the controller proposed in this paper based on an improved STM is compatible with system performance and system security, thereby further improving system reliability.

Remark 5. Different from the traditional periodic control method [35, 36], the ETC method executes tasks and transmits information only when needed, thus avoiding the consumption of computational and communication resources caused by periodic execution. According to Remark 3, utilizing the relatively simple structure of MTN-based controller can reduce the requirement for computing resources. To sum up, the MTN-based event-triggered controller developed in this paper can realize the control aims by lower resource consumption.

4. Simulation and analysis

In this section, an practical dynamic model is introduced to the feasibility and superiority of the proposed scheme.

4.1. Dynamic model

Consider a class of single-link manipulator system subject to motor dynamics, its schematic diagram can refer to [37] [Figure 6]. According to [37,38], its stochastic nonlinear system model with actuator and system external failures can be reformulated as

$$\begin{cases} d\chi_1 = \chi_2 dt \\ d\chi_2 = \left(\frac{1}{C}\chi_3 - \frac{N}{C}\chi_2 - \frac{D}{C}\sin(\chi_1)\right)dt + \frac{\mathrm{H}(\chi_1^2)}{C}d\vartheta \\ d\chi_3 = \left(\frac{\sum_{i=1}^{w} c_i\varphi_i(\chi)\left(\lambda_i\mu_{PFi}(t)+\mu_{TFi}\right)}{J} - \frac{K}{J}\chi_2 \right. \\ \qquad \left. - \frac{L}{J}\chi_3 + \Gamma(t)\,\mathrm{P}(\chi)\right)dt \\ y = \chi_1 \end{cases} \tag{64}$$

where χ_1, χ_2 and χ_3 denote the position, velocity, and acceleration of the link angular, respectively. The system variables are selected as $C = 1$ kg m^2, $N = 1$ Nms/rad, $m = 1$ kg m^2/s^2, $J = 1H$, $L = 0.5\Omega$, $K = 0.2$ Nm/A, $\mathrm{H}(\chi_1^2) = 0.1\sin(\chi_1^2)$, $\varphi_1(\chi) = 1.9 + 0.1\sin(\chi_1)$, $\varphi_2(\chi) = 1 + 0.2\sin(\chi_2)$, $\Gamma(t)$ is elaborated in (2), and the system external failure $\mathrm{P}(\chi) = 5\chi_2\sin(\chi_1)$. The reference signal $y_d = 0.5\sin(2t)$.

4.2. Control parameter selection

The initial state is chosen as $[\chi_1(0), \chi_2(0), \chi_3(0)]^{\mathrm{T}} = [0,0,0]^{\mathrm{T}}$. The initial values are given as $\hat{\boldsymbol{k}}(0) = [-1.5,0,0]^{\mathrm{T}}$ and $\bar{\mu}_{b1}(0) = \bar{\mu}_{b2}(0) = 0$. Furthermore, the designed parameters in the controller are given as $c_1 = 1$, $c_2 = 1$, $\beta_1 = 4$, $\beta_2 = 5$, $\beta_3 = 1$, $\beta = 10$, $\beta_k = 0.2$, $r_1 = 23$, $r_2 = 15$, $r_3 = 30$, $\mathrm{M}_1 = 2$, $\mathrm{M}_2 = 2$, $\mathrm{M}_3 = 0.5$, $\zeta = 0.1$, $\mathrm{T}_1 = 1$, $\mathrm{T}_2 = 25$, $\bar{\mathrm{M}} = 15$, $\eta = 0.1$.

4.3. Simulation study

Example 1. Actuator 1 abruptly loses 80% of its efficiency and Actuator 2 abruptly loses 50% of its efficiency, from 11 s; Actuator 1 and Actuator 2 abruptly lose 70% of its efficiency, from 18 s. All of them are PLOE failures. The system external failure abruptly occurs from 25 s.

Figs. 1–6 gives the simulation results of Example 1. Fig. 1 shows the curves of reference signal y_d and output signal y under proposed threshold mechanism compared with three threshold mechanisms called fixed, relative, and switching in [18]. Fig. 2 displays the curves of output signal tracking error under four strategies. Fig. 3 presents the curves of states χ_2 and χ_3 under proposed threshold strategy. Fig. 4 shows the controller outputs ϖ_1, ϖ_2 and actuator outputs $\mu_{\mathrm{b}1}$, $\mu_{\mathrm{b}2}$. The system external failure $\mathrm{P}(\chi)$ is plotted in Fig. 5. The triggering events are elaborated in Fig. 6. At the beginning, the amplitude of the controller output ϖ_1 and ϖ_2 are large so the controllers switch

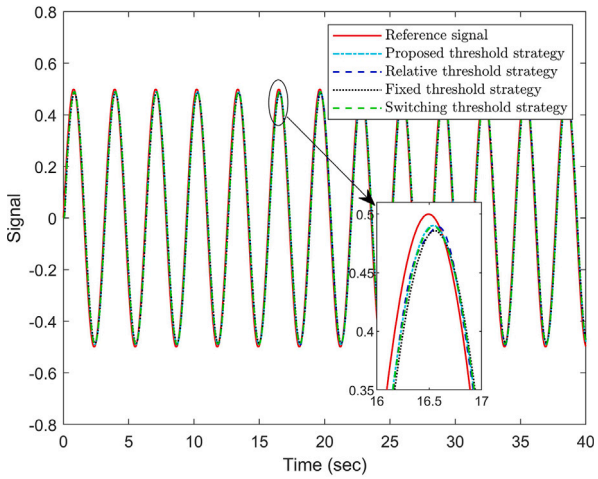

Fig. 1. Tracking control performance.

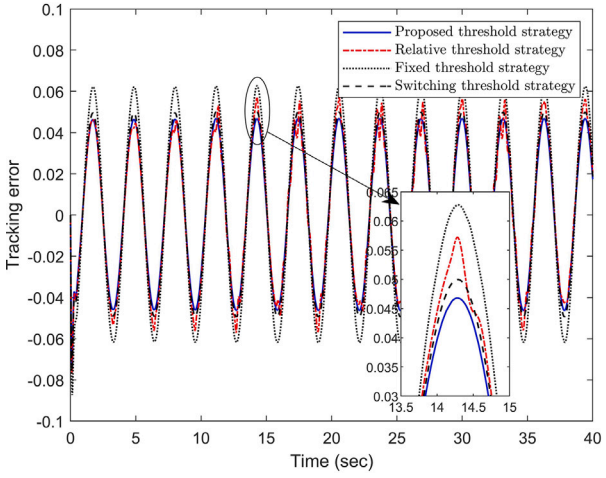

Fig. 2. The curves of output signal tracking error.

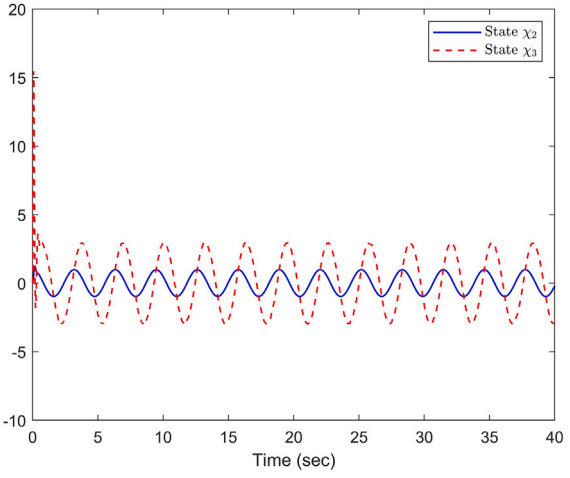

Fig. 3. The curves of states χ_2 and χ_3 under proposed threshold strategy.

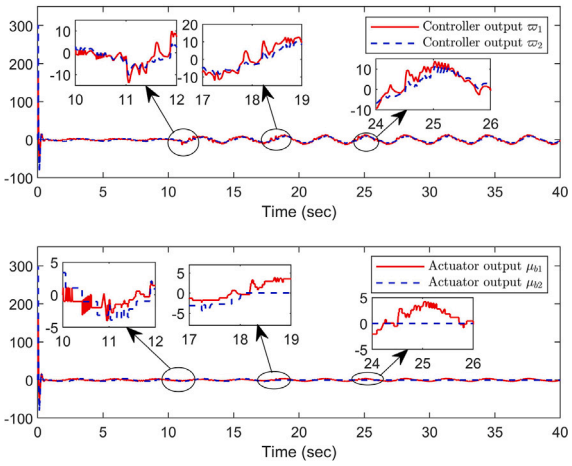

Fig. 4. The curves of controller outputs ϖ_1, ϖ_2 and actuator outputs μ_{b1}, μ_{b2} under proposed threshold strategy.

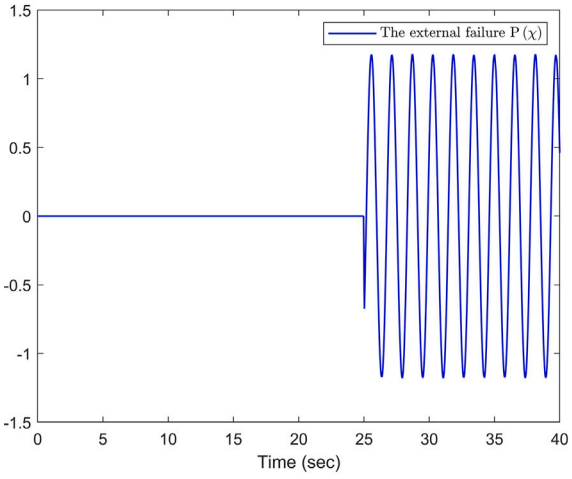

Fig. 5. The curve of system external failure P(χ) under proposed threshold strategy.

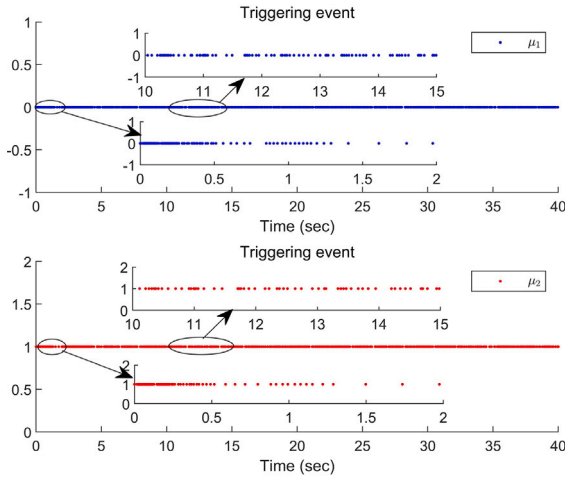

Fig. 6. The triggering events of μ_1 and μ_2 under proposed threshold strategy.

to the FTM, and when the controller output decrease to less than 25, the triggering mechanism is automatically switched to the RTM. Furthermore, we can see from Fig. 4 that when the failure occurs at

Table 1
Number of triggering events for Example 1.

Time	Actuator 1	Actuator 2
9–10 s	14	9
11–12 s	22	14
13–14 s	13	9
16–17 s	11	7
18–19 s	22	15
20–21 s	18	11
23–24 s	16	12
25–26 s	19	16
27–28 s	16	12

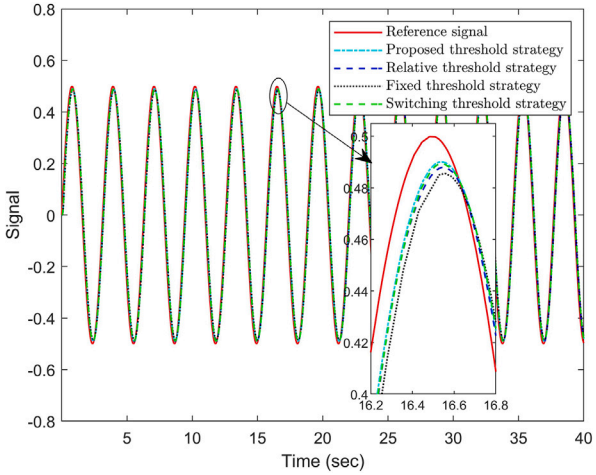

Fig. 7. Tracking control performance.

11 s, 18 s and 25 s, the proposed threshold strategy can switch between the trigger modes FTM and RTM according to the magnitude size of the controller and its rate of change.

To clearly demonstrate the ability of the proposed event-triggered fault-tolerant controller to compensate for failures, the times of triggering are given in Table 1 under proposed threshold strategy.

See Table 1, when Actuator 1 is subjected to 80% PLOE and Actuator 2 is subjected to 50% PLOE from 11 s, the times of triggering for Actuators 1 and 2 significantly increase at 11–12 s. Then, the actuator failures are compensated by the designed controller, so the times of triggering for Actuators 1 and 2 have reduced at 13–14 s. Similarly, when Actuators 1 and 2 fail from 18 s and system external failure occurs from 25 s, the times of triggering accordingly increase. After they decrease under the action of the controller.

Example 2. Actuator 1 is abruptly stuck, i.e., $\mu_{b1} = 0$, from 11 s; Actuator 2 abruptly loses 30% of its efficiency, from 11 s and loses its effectiveness of 40%, from 18 s. Among them, actuator failures include TLOE and PLOE failures. The system external failure abruptly occurs from 25 s.

The simulation results of Example 2 are shown in Figs. 7–12. Similarly, the times of triggering for Example 2 are given in Table 2.

See Table 2, when Actuator 1 is TLOE and Actuator 2 loses its effectiveness of 30%, which is PLOE failure, from 11 s, the times of triggering for Actuators 1 and 2 increase at 12–13 s. Then, due to the compensating influence of the controller, the times of triggering for Actuators 1 and 2 decline at 14–15 s. Similarly, when Actuator 2 is subjected to 40% PLOE from 18 s, and system external failure occurs from 25 s, the times of triggering also follow the same regularity.

Feasibility and superiority of the proposed control scheme to achieve the control aims is demonstrated, notwithstanding the controlled system undergoes actuator failures (PLOE or TLOE or both), abrupt system external failure and limited resource.

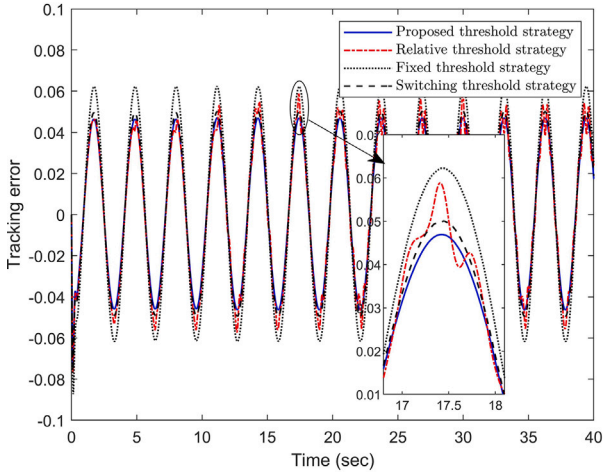

Fig. 8. The curves of output signal tracking error.

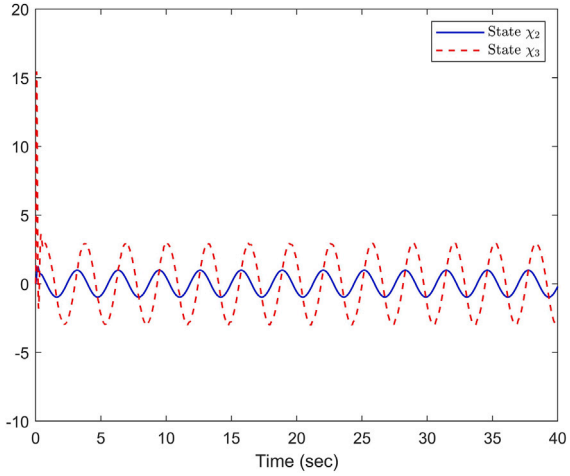

Fig. 9. The curves of states χ_2 and χ_3 under proposed threshold strategy.

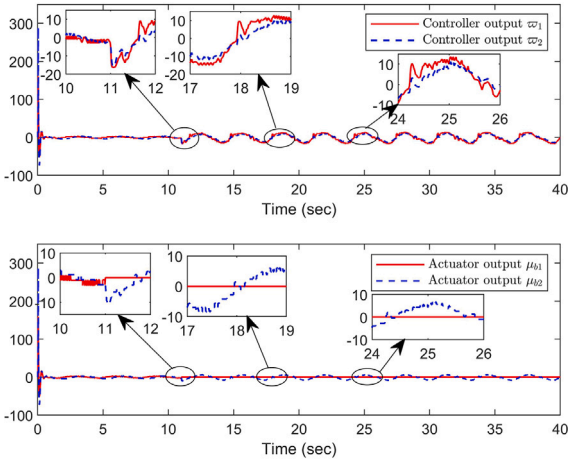

Fig. 10. The curves of controller outputs ϖ_1, ϖ_2 and actuator outputs μ_{b1}, μ_{b2} under proposed threshold strategy.

Remark 6. Considering that larger signal impulses in the ETM framework may pose challenges to system security, directly verifying this through simulation experiments is somewhat difficult. Therefore, we refer to the conclusions in [18], which indicate that larger signal impulses degrade the system's tracking performance. Based on this conclusion, by observing the tracking performance in Figs. 1–2 and Figs. 7–8, we can indirectly determine that the improved STM results in smaller signal impulses being applied to the system. Based on the fact that "smaller signal impulses applied to the system reduce the negative impact on system stability, thereby enhancing system security", we conclude that the system security under the improved STM framework is higher. Therefore, the mechanism proposed in this paper is more applicable to protect the regular operation of the system components under complex environments including actuator failure, external system failure, and other factors.

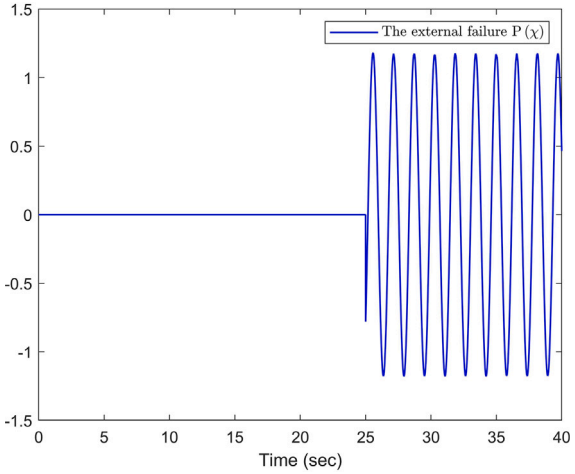

Fig. 11. The curve of system external failure P(χ) under proposed threshold strategy.

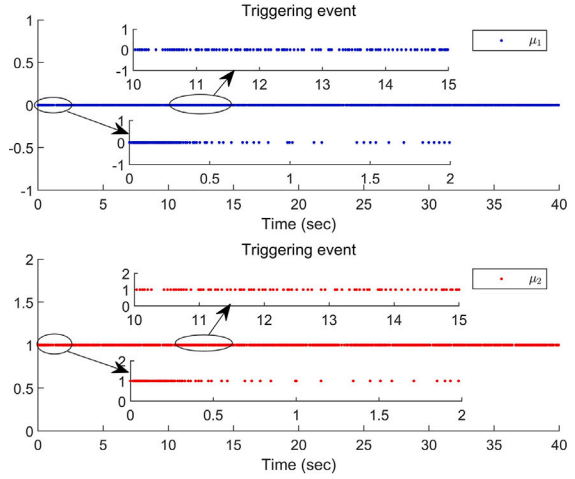

Fig. 12. The triggering events of μ_1 and μ_2 under proposed threshold strategy.

Table 2
Number of triggering events for Example 2.

Time	Actuator 1	Actuator 2
9–10 s	14	11
11–12 s	24	18
13–14 s	17	13
16–17 s	20	14
18–19 s	22	19
20–21 s	21	15
23–24 s	23	16
25–26 s	25	18
27–28 s	20	13

Remark 7. Theoretically speaking, decreasing the value of η and increasing the value of r_i can make the system have optimal tracking performance. Nevertheless, by observing (15) and (52), it can be noticed that the increasing r_i may result in an increase in the amplitude of the control signal. Hence, it is crucial to strike a delicate balance between tracking performance and control performance. By selecting appropriate design parameters, we can achieve superior control performance.

Remark 8. It can be seen from (6) and (39) that decreasing $\bar{M}$ i.e., decreasing M_1, M_2, M_3, ζ and T_2 improves the control performance of the system. However, the ETM (5) indicates that decreasing M_1, M_2, M_3, ζ and T_2 will result in the event triggering interval becoming shorter, which is not satisfactory in practical implementation. Therefore, the balance between control performance and internal communication transmission can be achieved by selecting the suitable parameters M_1, M_2, M_3, ζ and T_2. Furthermore, it can also be seen from (5) that if T_1 is increased, the large impulse may act on the system, thus leading to degradation of the control performance, and if T_1 is decreased, it will lead to an easy switching to the FTM, thus leading to degradation of the control performance. Thereby, the control performance of the system is ensured by selecting the appropriate parameter T_1.

5. Conclusion

In this paper, the problem of event-triggered adaptive control of stochastic nonlinear systems in the presence of abrupt system external failure and finite number of actuator failures including PLOE or TLOE is addressed. It has been demonstrated that the improved STM proposed in this paper can effectively overcome the system security hazards caused by overload impulses resulting from two types of failures and other factors, thereby indirectly enhancing the control performance of the system. Moreover, the proposed scheme achieves the control aims with lower resource consumption due to the simple structure of MTN. The effectiveness and superiority are also demonstrated on a third-order single-link manipulator through simulation. However, in practical engineering control, failures can occur indefinitely. In future work, we will focus on investigating the capability of the improved STM proposed in this paper to handle the more comprehensive actuator fault models presented in [31,32].

CRediT authorship contribution statement

Yang Du: Writing – original draft, Software, Methodology, Formal analysis. **Shan-Liang Zhu:** Writing – original draft, Supervision, Formal analysis. **Yu-Qun Han:** Writing – review & editing, Supervision, Methodology, Funding acquisition.

Declaration of competing interest

The authors declare that they have no known competing financial interests or personal relationships that could have appeared to influence the work reported in this paper.

Data availability

Data sharing is not applicable to this article as no datasets were generated or analyzed during the current study.

References

[1] Zhou J, Wen CY, Zhang Y. Adaptive backstepping control of a class of uncertain nonlinear systems with unknown backlash-like hysteresis. IEEE Trans Autom Control 2004;49(10):1751–9.
[2] Guerra TM, Aguiar B, Berdjag D, Demaya B. Robust estimation for nonlinear continuous-discrete systems with missing outputs: Application to automatic train control. IEEE Trans Control Syst Technol 2022;3(30):1304–10.
[3] Derakhshannia M, Moosapour SS. Disturbance observer-based sliding mode control for consensus tracking of chaotic nonlinear multi-agent systems. Math Comput Simulation 2022;194:610–28.
[4] Wang CR, Zhang L, Cao F. Inverse optimal control of a class of nonlinear multi-agent systems with applications to ship slew rate control. J Dyn Syst Meas Control 2022;144(7):74501–6.
[5] Wu ZJ, Xie XJ, Zhang SY. Adaptive backstepping controller design using stochastic small-gain theorem. Automatica 2007;43(4):608–20.
[6] Liu SJ, Zhang JF, Jiang ZP. Decentralized adaptive output-feedback stabilization for large-scale stochastic nonlinear systems. Automatica 2007;43(2):238–51.
[7] Li GF, Tian Y, Chen YH. Adaptive robust control for a class of stochastic nonlinear uncertain systems. IEEE Access 2020;8:51610–20.
[8] Wu J, Chen XM, Zhao QJ, Li J, Wu ZG. Adaptive neural dynamic surface control with prespecified tracking accuracy of uncertain stochastic nonstrict-feedback systems. IEEE Trans Cybern 2022;52(5):3408–21.
[9] Gao TT, Liu YJ, Li DP, Tong SC, Li TS. Adaptive neural control using tangent time-varying BLFs for a class of uncertain stochastic nonlinear systems with full state constraints. IEEE Trans Cybern 2021;51(4):1943–53.
[10] Wang N, Tao FZ, Fu ZM, Song SZ. Adaptive fuzzy control for a class of stochastic strict feedback high-order nonlinear systems with full-state constraints. IEEE Trans Syst Man Cybern A 2022;1(52):205–13.
[11] Han YQ, Yan HS. Adaptive multi-dimensional Taylor network tracking control for SISO uncertain stochastic non-linear systems. IET Control Theory Appl 2018;12(8):1107–15.
[12] He WJ, Han YQ, Li N, Zhu SL. Novel adaptive controller design for a class of switched nonlinear systems subject to input delay using multi-dimensional Taylor network. Internat J Adapt Control Signal Process 2022;36(3):607–24.
[13] He WJ, Zhu SL, Li N, Han YQ. Adaptive finite-time control for switched nonlinear systems subject to multiple objective constraints via multi-dimensional Taylor network approach. ISA Trans 2023;136:323–33.
[14] He WJ, Zhu SL, Lu LT, Han YQ. A novel network-based adaptive fault-tolerant control of switched nonlinear systems subject to multiple faults under prescribed performance. ISA Trans 2024;145:78–86.
[15] Du Y, Zhu SL, Han YQ. Event-triggered adaptive multi-dimensional Taylor network tracking control for stochastic nonlinear systems. Trans Inst Meas Control 2024;46(1):193–203.
[16] Wang HQ, Xu K, Qiu JB. Event-triggered adaptive fuzzy fixed-time tracking control for a class of nonstrict-feedback nonlinear systems. IEEE Trans Circuits Syst I Regul Pap 2021;68(7):3058–68.
[17] Hu XY, Li YX, Hou ZS, Niu B. Event-triggered prescribed performance adaptive fuzzy asymptotic tracking of nonstrict-feedback nonlinear systems. Internat J Robust Nonlinear Control 2021;31(12):5776–95.
[18] Xing LT, Wen CY, Liu ZT, Su HY, Cai JP. Event-triggered adaptive control for a class of uncertain nonlinear systems. IEEE Trans Autom Control 2017;62(4):2071–6.
[19] Du Y, Zhu SL, Zhai LL, Han YQ. Switching threshold-based event-triggered adaptive asymptotic tracking control for stochastic nonlinear systems with full-state constraints. Internat J Robust Nonlinear Control 2023;33(13):7908–28.
[20] Ma XS, Yang L, Ma LR, Yang F, Dong WH, Zhang L, et al. Distributed neuroadaptive monitoring fault-tolerant consensus control for nonlinear multi-agent systems with actuator faults. Internat J Robust Nonlinear Control 2022;32(9):5350–78.
[21] Sun Y, Shi P, Lim CC. Adaptive consensus control for output-constrained nonlinear multi-agent systems with actuator faults. J Franklin Inst 2022;359(9):4216–32.
[22] Ma JL, Park JH, Xu SY. Global adaptive control for uncertain nonlinear systems with sensor and actuator faults. IEEE Trans Syst Man Cybern A 2021;51(9):5503–10.
[23] Bounemeur A, Chemachema M. Adaptive fuzzy fault-tolerant control for a class of nonlinear systems under actuator faults: Application to an inverted pendulum. Int J Robot Control Syst 2021;1(2):102–15.
[24] Wang P, Yu CP, Sun J. Decentralized adaptive tracking control for nonlinear large-scale systems with unknown control directions. Internat J Robust Nonlinear Control 2022;32(2):620–48.
[25] Sheng N, Ai ZD, Tang J. Fuzzy adaptive command filtered backstepping fault-tolerant control for a class of nonlinear systems with actuator fault. J Franklin Inst 2021;358(13):6526–44.
[26] Pan HH, Zhang D, Sun WC, Yu XH. Event-triggered adaptive asymptotic tracking control of uncertain MIMO nonlinear systems with actuator faults. IEEE Trans Cybern 2022;52(9):8655–67.
[27] Wang JH, Liu Z, Chen CLP, Zhang Y. Event-triggered fuzzy adaptive compensation control for uncertain stochastic nonlinear systems with given transient specification and actuator failures. Fuzzy Sets and Systems 2019;365(15):1–21.

[28] Chen M, Liu XP, Wang HQ. Adaptive robust fault-tolerant control for nonlinear systems with prescribed performance. Nonlinear Dynam 2015;81(4):1727–39.
[29] Wang HQ, Bai W, Liu PX. Finite-time adaptive fault-tolerant control for nonlinear systems with multiple faults. IEEE/CAA J Autom Sin 2019;6(6):1417–27.
[30] Wang MX, Zhu SL, Liu SM, Du Y, Han YQ. Design of adaptive finite-time fault-tolerant controller for stochastic nonlinear systems with multiple faults. IEEE Trans Autom Sci Eng 2023;20(4):2492–502.
[31] Zhang CL, Guo G. Prescribed performance fault-tolerant control of nonlinear systems via actuator switching. IEEE Trans Fuzzy Syst 2024;32(3):1013–22.
[32] Yang QM, Ge SS, Sun YX. Adaptive actuator fault tolerant control for uncertain nonlinear systems with multiple actuators. Automatica 2015;60:92–9.
[33] Liu Z, Wang JH, Chen CLP, Zhang Y. Event trigger fuzzy adaptive compensation control of uncertain stochastic nonlinear systems with actuator failures. IEEE Trans Fuzzy Syst 2018;26(6):3770–81.
[34] Deng H, Miroslav K, Williams RJ. Stabilization of stochastic nonlinear systems driven by noise of unknown covariance. IEEE Trans Autom Control 2001;46(8):1237–53.
[35] Heffernan D, Leen G. A time-triggered control network for industrial automation. Assem Autom 2002;22(1):60–8.
[36] Schild K, Würtz J. Scheduling of time-triggered real-time systems. Constraints 2000;5(4):335–57.
[37] Wu CW, Liu JX, Xiong YY, Wu LG. Observer-based adaptive fault-tolerant tracking control of nonlinear nonstrict-feedback systems. IEEE Trans Neural Netw Learn Syst 2018;29(7):3022–33.
[38] Wang LJ, Chen CLP. Reduced-order observer-based dynamic event-triggered adaptive NN control for stochastic nonlinear systems subject to unknown input saturation. IEEE Trans Neural Netw Learn Syst 2021;32(4):1678–90.